A new method for estimating the conductive filament temperature in OxRAM devices based on escape rate theory

A. Rodriguez-Fernandez, J. Muñoz-Gorriz, J. Suñé, E. Miranda

Departament d'Enginyeria Electrònica, Universitat Autònoma de Barcelona, Cerdanyola del Valles, 08193, Spain

Abstract

Because of the atomic nature of the system under study, an estimation of the temperature of the conductive filament (CF) in OxRAM devices as a function of the applied bias can only be obtained by means of indirect methods, usually electrothermal simulations. In this paper, a heuristic approach that combines time-dependent dielectric breakdown (TDDB) statistics for the electroformed device with field and temperature-assisted ionic transport within the framework of escape rate theory is presented. Extended expressions for the time-to-failure acceleration law (*E*-model) and for the Kramers' rate compatible both with the standard models at moderate/high biases and with the principle of detailed balance at equilibrium are proposed. An approximate expression for the CF temperature is reported. For the investigated stress voltage range (0.30V-0.65V), the estimated CF temperature at the SET condition is found to be in the range 350K-600K.

Keywords: resistive switching, oxide breakdown, memristor, OxRAM

Email corresponding author: enrique.miranda@uab.cat

1. Introduction

OxRAM (Oxide-based Random Access Memory) is a serious candidate for the next generation of non-volatile memory devices and neuromorphic circuits [1]. Basically, its operating principle consists in the formation and dissolution of a section (or gap) in a metal or oxygen vacancy pathway (the conducting filament) spanning the oxide film in a MIM structure. These two states are often referred to as the low (LRS) and high (HRS) resistance states, respectively, and they correspond to one bit of information. While the electron current magnitude is associated with the read operation, ion displacement is the basis for the erase (RESET) and write (SET) processes. This technology has demonstrated high switching speed, endurance, scalability, low power consumption, and integration feasibility in the form of 3D stacks [2]. However, its ultimately success will rely on a deep understanding of the many physical factors affecting its performance and reliability. One of these factors that still remains vaguely defined because of the local and atom-sized nature of the problem is the temperature associated with the formation (SET) of the CF. Several works have contributed to get insight into the role played by temperature in the SET and RESET processes of OxRAM devices, the vast majority based on solving the heat equation with charge transport within a classical framework [3-5]. The identification of the device/environment temperature with the CF temperature is also an issue that demands attention. In this work, a heuristic approach that combines a phenomenological model (time-to-failure acceleration law) with a very fruitful theory which is at the heart of many scientific disciplines including physics, chemistry, engineering, and biology: the transition or escape rate theory, is proposed for estimating the CF temperature. As it will be discussed here, both formulations share a common origin but are

not fully equivalent. The idea of noise-activated escape from a metastable state, masterly developed by Kramers following the pioneering works of Arrhenius and many others [6,7], establishes that a (fictitious) particle located at the bottom of a potential well, which accounts for the action of a field of force, may have enough energy because of thermal agitation to escape over the saddle point of a potential barrier. At the end, this can represent a chemical bond breakage or the diffusive movement (hopping) of atomic species in a tilted periodic potential. The minimum energy required to overcome the barrier separating the initial and final states is called the activation energy E_A. Temperature comes into play from the Langevin equation and the fluctuation-dissipation theorem. In rate theory, the possibility of recrossings of the saddle point is often neglected because of a marked asymmetry in the transition processes. However, expressions that obey the principle of detailed balance [6], a relevant feature for a successful comparison between both approaches (acceleration law and escape rate theory), are shown to be necessary when the system is close to the equilibrium point, *i.e.* when $V \rightarrow 0$V.

2. Experimental data and conventional approach

The devices used for this investigation are 1T1R structures. The switching cell consists in a 10nm-thick HfO_2 film deposited by ALD and sandwiched between TiN and Ti electrodes. The cell is connected in series with an NMOS transistor. Current, voltage and time (*I-V-t*) measurements were performed using a Keithley 4200-SCS semiconductor parameter analyzer combined with a 4225-RPM pulse generator unit. Figure 1 illustrates typical bipolar switching behavior (50cycles@50Vs^{-1}). The transistor is used to limit the damage that suffers the

switching cell during the SET process. The heavy solid line corresponds to the median *I-V* curve. The device was previously electroformed with V_F=4V. Notice, from Fig.1, that SET and RESET voltages are symmetrically located at 0.5V and -0.5V, respectively, which indicates a common triggering mechanism. The LRS↔HRS transition rates are different which points out an asymmetry in the reduction-oxidation dynamics as the voltage changes.

Figure 2 shows constant-voltage stress (CVS) measurements performed at different positive voltages on a single electroformed device. The device is initially in HRS (CF with gap) and is recovered from LRS (CF without gap) using a negative voltage ramp passing the RESET point. Because of this, two sources of randomness affect the experimental data: first, one related to the cycle-to-cycle variations in the morphology of the CF, and second, one related to the TDDB statistics inherent to the breakdown process of the gap region. Figure 3.a shows multiple *Weibits* for the SET time (τ) associated with CVS experiments. Each data set for *V*=0.45, 0.50, 0.55, 0.60, 0.65V consists in 100 cycles [8]. In this work, additional measurements were performed at *V*=0.30, 0.35, 0.40V. Notice that for these latest values, data sets are reduced because of the longer time required for completing the experiments and because of the uncertainty in the determination of τ (*I-t* curves show progressive degradation). Uniform acceleration is observed with an average shape factor β=1.17. Figure 3.b shows that the phenomenological exponential TF (time-to-failure) model:

$$\tau = \tau_F exp(-\gamma V) \quad (1)$$

where

$$\tau_F = \tau_0[-ln(1-F)]^{1/\beta} \quad (2)$$

closely agrees with the experimental data for different cumulative fractions (F). The fitting constants are τ_0=3.46·10^{7}s and γ=47.6V^{-1} (voltage acceleration factor). This is the standard approach for reliability analysis of thin oxides often linked to the thermochemical model (E-model) [9,10]. However, notice that Eq. (1) yields a long yet finite τ for V=0, which is rather questionable (recall that thermal noise is always present). We can approximately associate $\tau(F=0.5)$ (Eq. (2)) with the mean passage time over the activation barrier. Now, we turn the attention to Kramers' escape rate theory which expresses the passage time as:

$$\tau = \tau_0' exp\left(\frac{E_A - e\alpha V}{k_B T}\right) \quad (3)$$

where τ_0'=1.43·10^{-14}s is the inverse of the Hf-O bond vibration frequency [11], E_A=1.25eV for HfO_2 [12], $0 \leq \alpha \leq 1$ a lowering barrier factor, and k_BT the thermal energy. Eq. (3) expresses a reduction of the barrier height as the voltage increases and is valid as far as (E_A-$e\alpha V$)>> k_BT, where T is the temperature of the heat bath at the bottom of the well. The forward reaction or escape rate is defined as $k^+=\tau^{-1}$. It is clear that in order to reconcile Eqs.(1) and (3), T should increase as the voltage increases. Notice that Eqs. (1) and (3) are similar but not identical since T is absent in the former expression. This feature has been previously reported for thin films [13,14] and has been ascribed to the collaborative effect of many simultaneous reactions. In [9], γ is assumed to depend linearly on T, but no physical justification is

provided.

3. Extended models

Now we proceed to extrapolate the above expressions to the very low voltage regime so as to make them compatible with the standard approaches (Eqs. (1) and (3)) at moderate/high bias and consistent with the principle of detailed balance at equilibrium, *i.e.* $\tau(V\rightarrow 0)\rightarrow\infty$. Eq. (1) becomes:

$$\tau = \tau_F \left\{ exp\left[\eta\frac{V}{\varepsilon}\right] - exp\left[-(1-\eta)\frac{V}{\varepsilon}\right]\right\}^{-1} \quad (4)$$

where $0\leq\eta\leq 1$ is a dimensionless factor that takes into account the possible asymmetry in the forward and backward transition rates [6] and ε is a constant. Taking $\eta/\varepsilon=\gamma$, Eq. (4) coincides with Eq. (1) in the limit $V/\varepsilon>>1$. As far as k_BT is associated with the thermal noise at the bottom of the wells, $\varepsilon/\eta=1/\gamma=0.021$V can be interpreted as the noise strength in a generalized potential V [7]. While Fig.4.a illustrates a process in which the system can go back and forth in the reaction coordinates (progress along a reaction pathway) of a symmetric double-well potential, Fig.4.b shows the case for a reaction occurring in a preferred direction (asymmetric transition). The particle here represents the free energy state of the system. The result of this extrapolation can be seen in Fig.5. Notice that τ largely increases at very low applied biases depending on the asymmetry (η) of the reactions. Although this behavior is qualitatively in agreement with previous reports [15], an alternative extrapolation law cannot be ruled out.

Following similar arguments ($k=k^+-k^-$), Eq. (3) can be extended as:

$$\tau = \tau_0' \left\{ exp\left[-\frac{E_A - e\alpha V}{k_B T} \right] - exp\left[-\frac{E_A + e(1-\alpha)V}{k_B T} \right] \right\}^{-1} \quad (5)$$

Eq. (5) is consistent with Crooks' theorem (fluctuation-dissipation theorem) for the ratio of the reaction rates [16]:

$$\frac{k^+}{k^-} = \frac{exp\left[-\frac{E_A - e\alpha V}{k_B T} \right]}{exp\left[-\frac{E_A + e(1-\alpha)V}{k_B T} \right]} = exp\left(\frac{eV}{k_B T} \right) \quad (6)$$

which states that the work performed in the transition is *eV* and the entropy production *eV/T*. Figures 4.c-d illustrate the transition process in spatial coordinates. While in equilibrium there is no preferred direction for the ion flow (see Fig.4.c), under nonequilibrium conditions (biased periodic potential), ion displacement is unidirectionally activated (see Fig.4.d). This latest process will ultimately fill the gap with oxygen vacancies leading the device to LRS. It is implicitly assumed that thermalization takes place after each ion jump leading to a memory loss effect (not to be confused with the memristive effect). Notice that Eq. (5) is widely used to describe the ion flow in OxRAM and CBRAM (conductive bridge) devices [17]. The ion current model is often identified with the Butler-Volmer equation [18,19], which is one of the most fundamental relationships in electrochemical kinetics. In this latest case, E_A is associated with the so-called overactivation potential and α with the charge transfer coefficient.

4. Results and conclusions

The central idea of our paper is that the CF temperature can be estimated matching Eqs.(4) and (5) and solving for *T*. Eq.(5) explicitly depends on *T* while Eq.(4) does not. In other words, we are looking for the temperature values that reconcile both approaches. To this end, identical extrapolation laws were assumed in Section 3. In general, the problem has to be solved numerically. The obtained results for some specific conditions are plotted in Figs. 5 and 6. As expected, as the voltage increases, the SET time decreases and the temperature at which this event occurs increases. Moreover, as illustrated in Fig.6, this behavior is fully consistent with the electrothermal model predictions [3,17]. *F* determines which percentile of the devices we are dealing with. For each voltage, there is a temperature range because of the different morphologies of the CF and gap region. Data dispersion is often neglected in electrothermal simulations. Notice that the extended models presented in Section 3 allows us to examine in detail the very low bias regime where no experimental data are available.

In order to achieve better insight into the model results, an approximate closed-form expression for the CF temperature can be obtained neglecting the backward reactions in Eqs. (4) and (5). In this case, the temperature reads:

$$T(V) = \frac{E_A - e\alpha V}{k_B\left[ln\left(\frac{\tau_F}{\tau'_0}\right) - \gamma V\right]} \tag{7}$$

which yields $T(0V)=297K$ for $F=0.5$ as expected for equilibrium conditions. A comparison with the numerical solution for $T(V)$ is shown in Fig.7. The difference is only significant for $V<0.1V$. The question is how good Eq. (7) is for calculating $T(0V)$ given that it arises from a partial description of the problem. If, for the sake of simplicity, symmetric transitions

(α=η=0.5) are considered in the extended expressions, the matching condition for V=0V reads:

$$-\frac{E_A}{k_B T} exp\left(-\frac{E_A}{k_B T}\right) = -\frac{2\tau_0' \gamma E_A}{e\tau_F} \tag{8}$$

whose solution is:

$$T(0\text{V}) = -\frac{E_A}{k_B W_{-1}\left(-\frac{2\tau_0' \gamma E_A}{e\tau_F}\right)} \tag{9}$$

From Eq. (9), T(0V)=302K for F=0.5 is found which is very close to the value obtained from Eq.(7). W_{-1} in Eq.(9) is one of the negative branches of the Lambert function [20], *i.e.* the solution of the transcendental equation $We^{W}=x$.

In summary, a heuristic model for estimating the CF temperature as a function of the applied voltage was proposed. The model combines a phenomenological law for the breakdown acceleration factor of thin dielectrics (the gap region in our case) with a well-known theoretical formulation, namely escape rate theory. Temperature is chosen so as to reconcile both approaches following extrapolation laws consistent with detailed balance. It is found that, without the additament of any special particularity, backward reactions are only relevant close to equilibrium conditions.

Acknowledgements

Project TEC2017-84321-C4-4-R, MINECO, Spain. Project WAKeMeUP, ECSEL-Joint Undertaking H2020. C. Cagli, CEA-LETI, for sample provision and helpful discussion.

References

[1] J. Joshua Yang, D. Strukov, D. Stewart, Memristive devices for computing, Nanotech 8, 13-24, 2013

[2] D. Ielmini, Resistive switching memories based on metal oxides: mechanisms, reliability and scaling, Semicond Sci Technol 31, 63002, 2016

[3] D. Ielmini, Modeling the universal set/reset characteristics of bipolar RRAM by field- and temperature-driven filament growth, IEEE Trans Elect Dev 58, 4309-4317, 2011

[4] D. Niraula, V. Karpov, Heat transfer in filamentary RRAM devices, IEEE Trans Elec Dev 64, 4106, 2017

[5] S. Pazos, F. Aguirre, E. Miranda, S. Lombardo, F. Palumbo, Comparative study of the breakdown transients of thin Al_2O_3 and HfO_2 films in MIM structures and their connection with the thermal properties of materials, J Appl Phys 121, 094102, 2017

[6] P. Hanggi, P. Talkner, H. Borkovec, Reaction-rate theory: fifty years after Kramers. Rev Mod Phys 62, 251, 1990

[7] E. Pollak, P. Talkner, Reaction rate theory: What is was, where is it today, and where is it going?, Chaos 15, 026116, 2005

[8] A. Rodriguez-Fernandez, C. Cagli, L. Perniola, J. Suñé, E. Miranda, Identification of the generation/rupture mechanism of filamentary conductive paths in ReRAM devices using oxide failure analysis, Mic Rel 76, 178, 2017

[9] J.W. McPherson, Reliability Physics and Engineering: Time-to-failure modeling, Springer, 2010.

[10] A. Rodriguez-Fernandez, C. Cagli, J. Suñé, E. Miranda, Switching voltage and time

statistics of filamentary conductive paths in HfO2-based ReRAM devices, IEEE Electron Dev Lett 39, 656-659, 2018

[11] A. McNaught, A. Wilkinson, Compendium of Chemical Terminology, 2nd ed. Oxford, U.K, 1997.

[12] P. Lorenzi, R. Rao, F. Irrera, Conductive filament evolution in HfO_2 resistive RAM device during constant voltage stress, Mic Rel 55, 1446-1449, 2015

[13] D. Hsu, M. Wang, J. Lee, P. Juan, Electrical characteristics and reliability properties of metal-oxide-semiconductor field-effect transistors with ZrO_2 gate dielectric, J. Appl. Phys 101, 094105, 2007

[14] F. Chiu, Thickness and temperature dependence of dielectric realiability characteristics in cerium dioxide thin film, IEEE Trans Elec Dev 57, 2719-2725, 2010

[15] S. Menzel, S. Trappenrtzhofen, R. Waser, I. Valov, Switching kinetics of electrochemial metallization memory cells, Phys Chem Phys 15, 6945-6952, 2013

[16] B. Cleuren, C. Van den Broeck, R. Kawai, Fluctuation and dissipation, C. R. Physique 8, 567-578, 2007

[17] X. Guan, S. Yu, H. Philip Wong, On the switching parameter variation of metal-oxide RRAM-Part I: Physical modeling and simulation methodology, IEEE Trans Elec Dev 59, 1172-1182, 2012

[18] K. Shin, Y. Kim, F. Antolinez, J. Ha, S. Lee, J. Park, Controllable formation of nanofilaments in resistive memories via tip-enhanced electric fields, Adv Eletron Mater, 1600233, 2016

[19] M. Bocquet, D. Deleruyelle, H. Aziza, C. Muller, J. Portal, T. Cabout, E. Jalaguier,

Robust compact model for bilpolar oxide-based resistive switching memories, IEEE Trans Elect Dev 61, 674-681, 2014.

[20] R. Corless, G. Gonnet, D. Hare, D. Jeffrey, D. Knuth, On the Lambert W function, Adv Comp Mathematics 5, 329-359, 1996

Figure captions

Fig. 1. Typical bipolar *I-V* characteristics with the corresponding formation (HRS) and dissolution (LRS) of the gap region. SET and RESET points are also indicated.

Fig. 2. I-t characteristics for CVS experiments performed in the same device but at different voltages.

Fig. 3. (a) SET time (τ) distributions for CVS experiments. Symbols are experimental data. Solid lines are fitting results. *F* is the cumulative probability. (b) τ plotted as a function of the stress voltage for different *F* values.

Fig. 4. (a) and (b): Representation of the state transitions in terms of reaction coordinates. (c) and (d): Representation of the ion movement in spatial coordinates.

Fig. 5. SET time as a function of the applied voltage for different values of η (see Eq. (4)). Symbols are experimental data.

Fig. 6. Conducting filament temperature as a function of the applied voltage. T_0=295 K, V_{TH}/R=700K/V^2. A complete description of the electrothermal model can be found in [3].

Fig. 7. Comparison between numerical and approximate solutions for the CF temperature with different α values.

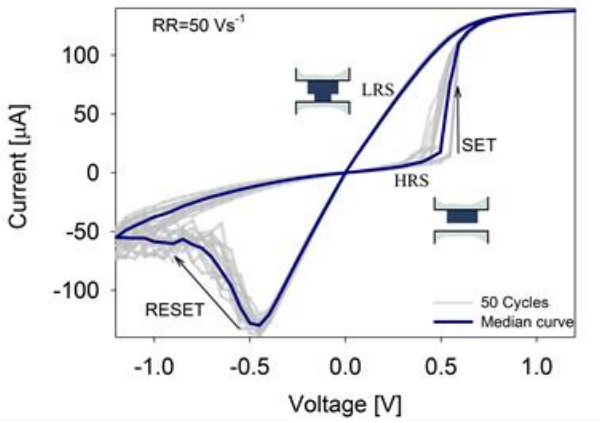
RR=50 Vs-1
100
50
0
-50
-100
Current [µA]
LRS
SET
HRS
RESET
50 Cycles
Median curve
-1.0
-0.5
0.0
0.5
1.0
Voltage [V]

FIGURE 1

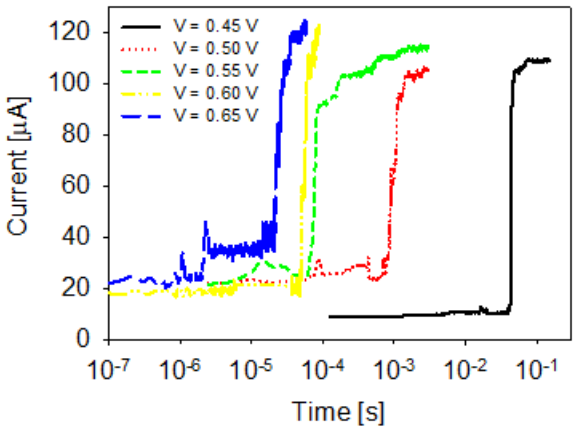
V = 0.45 V
V = 0.50 V
V = 0.55 V
V = 0.60 V
V = 0.65 V
Current [µA]
120
100
80
60
40
20
0
10-7
10-6
10-5
10-4
10-3
10-2
10-1
Time [s]

FIGURE 2

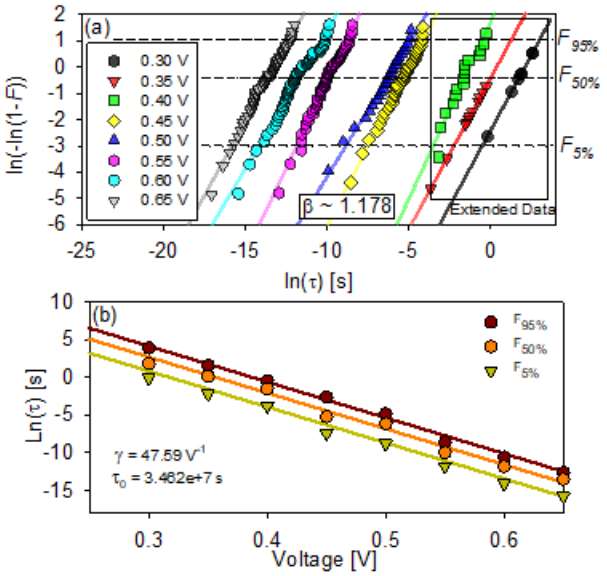
(a)
0.30 V
0.35 V
0.40 V
0.45 V
0.50 V
0.55 V
0.60 V
0.65 V
β ~ 1.178
Extended Data
F95%
F50%
F5%
ln(-ln(1-F))
ln(τ) [s]
(b)
Ln(τ) [s]
γ = 47.59 V-1
τ0 = 3.462e+7 s
Voltage [V]

FIGURE 3

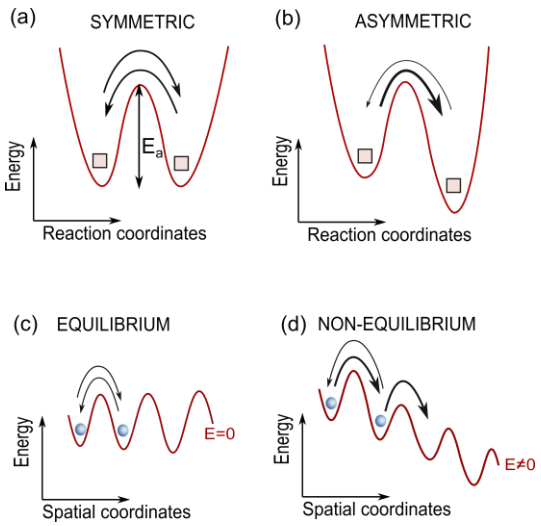
(a)
SYMMETRIC
Energy
E_a
Reaction coordinates
(b)
ASYMMETRIC
Energy
Reaction coordinates
(c)
EQUILIBRIUM
Energy
E=0
Spatial coordinates
(d)
NON-EQUILIBRIUM
Energy
E≠0
Spatial coordinates

FIGURE 4

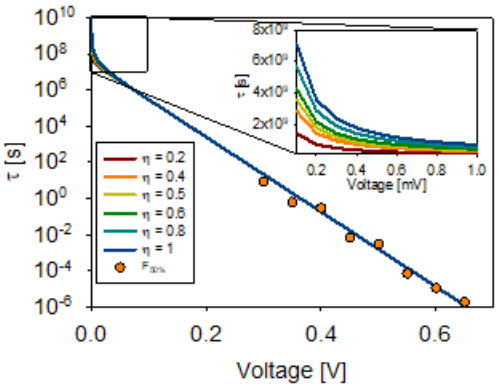

FIGURE 5

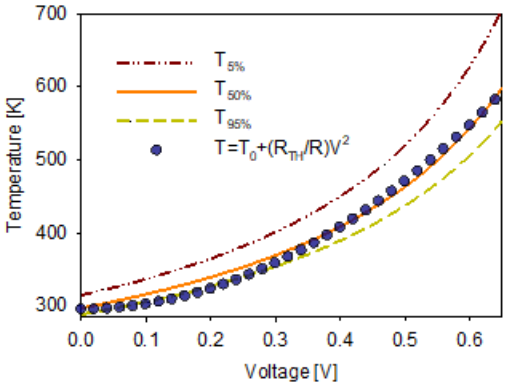
700
600
500
400
300
Temperature [K]
0.0
0.1
0.2
0.3
0.4
0.5
0.6
Voltage [V]
T5%
T50%
T95%
T=T0+(RTH/R)V2

FIGURE 6

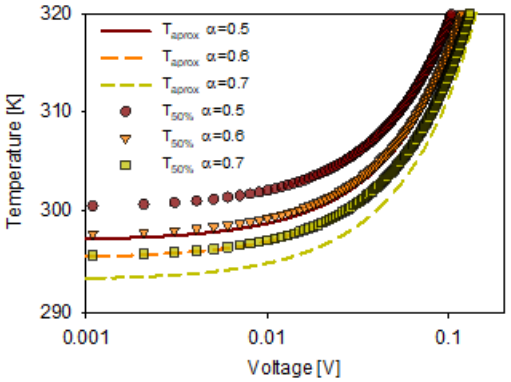
320
310
300
290
Temperature [K]
0.001
0.01
0.1
Voltage [V]
T aprox α=0.5
T aprox α=0.6
T aprox α=0.7
T 50% α=0.5
T 50% α=0.6
T 50% α=0.7

FIGURE 7